Rapid Communications

Tuning stoichiometry and its impact on superconductivity of monolayer and multilayer FeSe on $SrTiO_3$

Chong Liu and Ke Zou*

Department of Physics & Astronomy, University of British Columbia, Vancouver, British Columbia, Canada V6T 1Z1 and Quantum Matter Institute, University of British Columbia, Vancouver, British Columbia, Canada V6T 1Z4

(Received 4 February 2020; revised manuscript received 17 March 2020; accepted 18 March 2020; published 10 April 2020)

Synthesis of monolayer FeSe on $SrTiO_3$, with greatly enhanced superconductivity compared to bulk FeSe, remains difficult. Lengthy annealing within a certain temperature window is always required to achieve superconducting samples as reported by different groups around the world, but the mechanism of annealing in inducing superconductivity has not been elucidated. We grow FeSe films on $SrTiO_3$ by molecular beam epitaxy and adjust the stoichiometry by depositing additional small amounts of Fe atoms. The monolayer films become superconducting after the Fe deposition without annealing, and show similar superconducting transition temperatures as those of the annealed films in transport measurements. We also demonstrate on the 5-unit-cell films that the FeSe multilayer films can be reversibly tuned between the nonsuperconducting $\sqrt{5} \times \sqrt{5}$ phase with Fe vacancies and the superconducting 1×1 phase. Our results reveal that the anneal process in essence removes Fe vacancies and the additional Fe deposition serves as a more efficient way to achieve superconductivity. This work highlights the significance of stoichiometry in the superconductivity of FeSe thin films and provides an easy path for superconducting samples.

DOI: 10.1103/PhysRevB.101.140502

FeSe, with the simplest structure and chemical composition among Fe-based superconductors, has been intensely studied in the past decade [1]. It distinguishes itself in various aspects and poses many open questions. Bulk tetragonal FeSe has a superconducting transition temperature $T_c \approx 8$ K [2]. Monolayer tetragonal FeSe grown on $SrTiO_3$ (STO) shows greatly interface-enhanced superconductivity with T_c up to 65 K [3–5], albeit only after a long postannealing process. Efforts have been focused on understanding the mechanisms of enhanced superconductivity [6–9], since this may lead the way to the design of new superconductors with higher T_c.

High-T_c superconducting FeSe thin films are mostly grown by molecular beam epitaxy (MBE). A Se-rich condition is employed with the flux ratio Φ_{Se}:Φ_{Fe} ranging from 5 to 20, with a substrate temperature well above the evaporation temperature of Se [6,10,11]. Ideally, FeSe grown this way should be stoichiometric with Fe:Se = 1 : 1, but the long postgrowth annealing process required to reach superconducting states suggests otherwise [12,13]. Although stoichiometry has been difficult to characterize in FeSe thin films, it does affect the properties of bulk FeSe substantially. There exist multiple bulk phases of FeSe such as hexagonal α-Fe_xSe, tetragonal β-Fe_xSe, and hexagonal γ-Fe_7Se_8 [14,15], among which only the β phase is superconducting when $x \approx 1$ [15,16]. Almost defect-free β-FeSe single crystals have been obtained with $T_c \sim 10$ K [17,18]. Depending on the synthesis conditions, Fe vacancies or excess Fe atoms could exist in the bulk crystals and suppress the superconductivity. Substantially more Fe vacancies in β-Fe_xSe lead to other ordered crystal forms such as Fe_3Se_4, Fe_4Se_5, and Fe_9Se_{10} [19].

Because of the high Se flux used in MBE growth, the existence of excess Fe atoms or Se vacancies in FeSe thin films becomes unlikely. The presence of Fe vacancies may lead to the nonsuperconducting as-grown films. Revealed by *in situ* scanning tunneling microscopy (STM), the as-grown FeSe films on STO have high density of dumbbell-like defects and an insulating energy gap. With annealing, these defects are reduced, the film becomes metallic, and a superconducting gap opens up at Fermi energy [10,12,20,21]. A similar observation has been made on FeSe films on graphene as well, although the superconducting gaps are different [11,21]. Density functional theory calculations have attributed these dumbbell-like defects to Fe vacancies and claimed that they can diffuse between Fe sites during annealing and eventually move to the edges of the film [21]. Opposite observations include a recent STM work reporting an increase of FeSe film coverage after depositing additional Se at a low temperature, suggesting ~20% excess Fe in their films [22]. In addition, one scanning transmission electron microscope work shows the existence of interstitial Se atoms between FeSe and STO, although not in the FeSe itself [23], raising further questions about stoichiometry in few-layer FeSe films. The lack of direct experimental evidence makes it difficult to pin down how the stoichiometry affects the superconducting transition in FeSe films.

In this work, we grow few-unit-cell (UC) FeSe films on STO and deposit small amounts of additional Fe onto the as-grown films. Adding the Fe atoms substantially improves the film quality and induces superconductivity without a

*kzou@phas.ubc.ca

 ©2020 American Physical Society

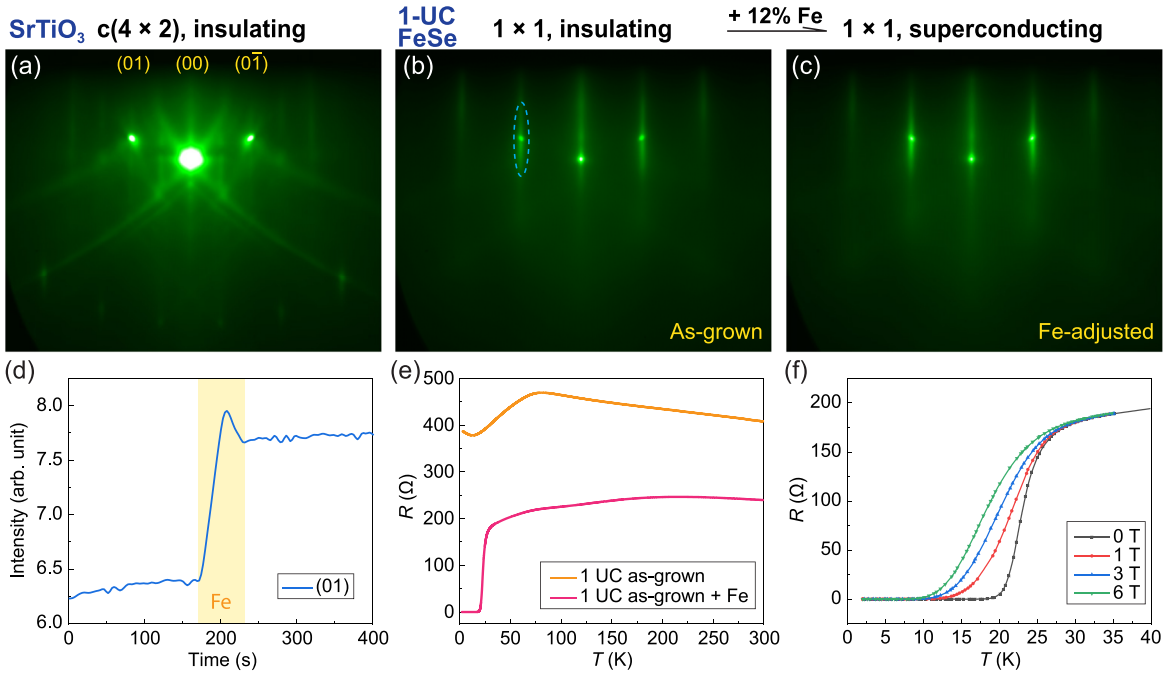

FIG. 1. (a) Reflection high-energy electron diffraction (RHEED) image of $SrTiO_3$ substrate with incident beam along the [100] direction. (b) and (c) RHEED images of as-grown 1-UC FeSe film and the same sample after Fe deposition, respectively. (d) Integrated intensity of the (01) diffraction streak as a function of time. The monitored areas are marked by the dashed ellipse in (b). The yellow interval indicates the period of Fe deposition. (e) Temperature dependence of the resistance of as-grown and Fe-adjusted monolayer FeSe films. (f) Temperature dependence of the resistance of Fe-adjusted monolayer FeSe film at low temperature with different out-of-plane magnetic field.

postanneal process. This approach serves as an alternative, easy, and time-saving method compared to the many hours of annealing required in the past. The T_c of monolayer FeSe on STO by this method can reach as high as the annealed samples in transport measurements, directly indicating that the as-grown FeSe films possess Fe vacancies in their layer structure. In a 5-UC sample, we control the surface reconstruction and stoichiometry by alternating deposition of Se and Fe and switch the FeSe multilayer between a Fe-vacancy phase and the superconducting phase.

FeSe films were grown on treated undoped STO substrates (CrysTec GmbH), using procedures similar to other groups [12,24,25]. The base pressure of the MBE chamber was $\sim 1 \times 10^{-10}$ Torr. The flux ratio was Φ_{Se}:$\Phi_{Fe} \approx 5$. The substrate temperature was 420 °C for growth and 480 °C for anneal. The samples were monitored by reflection high-energy electron diffraction (RHEED). The growth rate was ~0.2 UC/min, determined by RHEED intensity oscillation [26]. RHEED pattern simulations were generated by a program written in Wolfram *Mathematica*. For transport measurements, samples were capped by 12-UC FeTe grown at 280 °C following standard procedures [24]. Transport measurements were carried out in a Quantum Design physical property measurement system with the four-terminal method. Gold wires were bonded on the samples with indium lumps as the electrodes.

Figures 1(a) and 1(b) show the typical RHEED images of STO and as-grown monolayer FeSe grown at 420 °C, respectively. The FeSe film has a 1 × 1 square structure with lattice constant $a = 3.85$ Å, calibrated by the distance between diffraction streaks. Unlike the usual routine of annealing at higher temperature in ultrahigh vacuum for many hours, we kept the film at the growth temperature 420 °C, and deposited Fe atoms onto it. The RHEED intensity increased as shown in Figs. 1(c) and 1(d). It reached the maximum in 37 s and then decreased, and we stopped the Fe deposition [shaded area in Fig. 1(d)]. Both (01) and (00) diffraction streak intensities showed a similar trend with deposition; especially the (01) was increased by 24%. The RHEED intensity was enhanced without any sign of new phases or reconstructions, indicating that the as-grown film contained disordered Fe vacancies and the subsequently deposited Fe improved the stoichiometry and the overall quality of the film. Once the optimal stoichiometry was reached, which corresponded to the maximum intensity, additional Fe atoms started to accumulate on the surface and lower the RHEED intensity.

The extreme sensitivity of RHEED to the surface crystal structures allows us to capture small changes in the amount of Fe vacancies in the film. Taking the maximum of RHEED intensity as the indication of correct stoichiometry, we estimate the Fe-vacancy fraction δ in as-grown $Fe_{1-\delta}Se$ film by the deposition time: $\delta = t_{Fe}/(t_{FeSe} + t_{Fe}) = 0.12$, where t_{FeSe} and t_{Fe} are the Fe-Se codeposition time and the Fe deposition time before the maximal intensity [Fig. 1(d)], respectively, with the same Fe flux. The estimated Fe-vacancy fraction δ varies between different monolayer samples and ranges from 0.07 to 0.16 in our experiments.

The films were cooled down to 280 °C right after the Fe deposition and capped with 12-UC FeTe. Figure 1(e) shows the transport measurement results of a typical as-grown sample and the Fe-adjusted sample. The as-grown sample only showed the typical structural and antiferromagnetic transition of the FeTe capping layer at 80 K [27] and an insulating

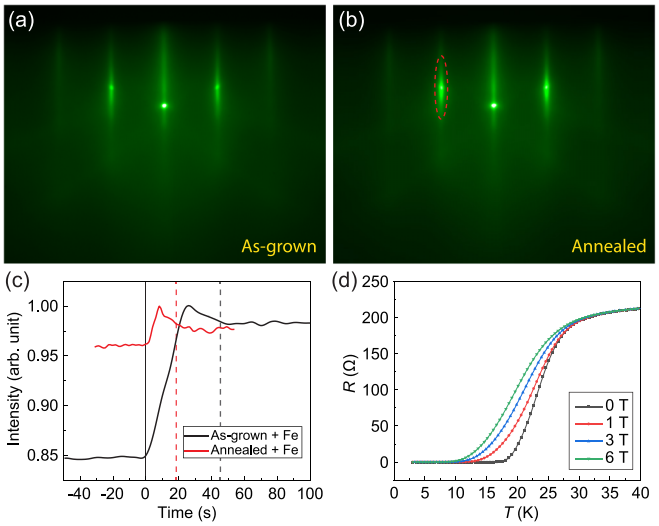

FIG. 2. (a) and (b) RHEED images of as-grown and annealed 1-UC FeSe film, respectively. (c) Integrated intensity of the (01) diffraction streak of the annealed film in (b) (red) and an as-grown 1-UC film (black) as a function of time during Fe deposition. For each curve, the maximal intensity is rescaled to 1 and the starting time of Fe deposition is reset to 0. Each dashed line indicates the end time of Fe deposition for the curve with the corresponding color. (d) Temperature dependence of the resistance of the FeSe film in (b) after Fe deposition, with different out-of-plane magnetic field.

behavior below 15 K, while the Fe-adjusted sample was more conductive and exhibited a superconducting transition. Closer observation in the low-temperature range shown in Fig. 1(f) gives the transition temperatures $T_c^{\text{onset}} = 31$ K, $T_c^{\text{mid}} = 23$ K, and $T_c^0 = 18$ K, similar to other groups' results of annealed samples [12,13,23]. The T_c shifted to lower temperatures when an external magnetic field was applied, as a result of the Meissner effect in a superconductor. We conclude that enhanced superconductivity in monolayer FeSe/STO can be achieved solely by increasing Fe content.

To compare, we prepared another monolayer sample (Fig. 2) and applied the standard annealing process at 480 °C for 3 h. As shown in Figs. 2(a) and 2(b), the RHEED intensity increased after annealing, manifesting the improvement of the crystal quality. To calculate the Fe-vacancy content in the annealed sample, we deposited Fe at 420 °C and carried out the same analysis method used in Fig. 1(d). The time to reach the maximal RHEED intensity was only 8 s and the relative increase of the intensity was <5% [red curve in Fig. 2(c)], much less than those for the as-grown samples [black curve in Fig. 2(c)], indicating the annealed film contained a lower Fe-vacancy fraction ($\delta \approx 0.02$). As shown in Fig. 2(d), the transport results are quite similar to those of the merely Fe-adjusted samples, with $T_c^{\text{onset}} = 33$ K, $T_c^{\text{mid}} = 23$ K, and $T_c^0 = 16$ K.

We have shown both annealing and Fe deposition can induce superconductivity in FeSe films with similar transition temperatures. Either method reduces the Fe vacancies that are commonly generated during the MBE growth procedures, and eventually leads to stoichiometric films. However, adding Fe atoms is more efficient compared to the typical several to tens of hours annealing that is required. Note that the scenario of Se richness may exist in as-grown films with the excess Se atoms mainly embedded in the $FeSe_{1+y}$ films, which is equivalent to Fe vacancies. Extra free Se atoms above FeSe lattices can hardly stay at the growth temperature of 420 °C.

The Fe adjustment approach was further examined by RHEED studies on multilayer films. Reconstructed surface structures provide a good indication of the existence of defects such as Fe vacancies, and their evolution can be easily tracked and characterized by RHEED. We utilized the $(\sqrt{5} \times \sqrt{5})$-$R26.6^\circ$ reconstruction that can be generated on thicker FeSe films to guide our experiments on multilayer films. Heavily Se-rich multilayer FeSe may show either $\sqrt{5} \times \sqrt{5}$ or $\sqrt{5} \times \sqrt{10}$ reconstructions [10,11,28], and the corresponding films are both insulating. STM studies have shown that the $\sqrt{5} \times \sqrt{5}$ reconstructions consist of ordered dumbbell-like defects which are suggested to be Fe vacancies by theoretical calculations [11,21].

We deposited a 5-UC FeSe film that was 1 × 1 as grown, and then intentionally introduced $(\sqrt{5} \times \sqrt{5})$-$R26.6^\circ$ reconstruction by annealing the film under Se flux at 250 °C for 5 min [Figs. 3 and 4(a)]. This temperature is above the evaporation temperature of Se, so most of Se will reevaporate from the surface, while a small number of Se atoms diffuse into the film and drive the whole film to the $\sqrt{5} \times \sqrt{5}$ structure with more Fe vacancies. As shown in Figs. 3(a) and 3(b), new diffraction streaks emerged in addition to the original 1 × 1 FeSe. By assuming a 1 × 1 square lattice with two $\sqrt{5} \times \sqrt{5}$ reconstructions which are rotated by ±26.6° with respect to the 1 × 1 lattice, the computer simulations of the RHEED patterns [Figs. 3(c) and 3(d)] agree well with the experimental results in both the [100] and the [110] directions. One candidate for the $\sqrt{5} \times \sqrt{5}$ structure is the Fe_4Se_5 phase, in which 20% Fe vacancies are arranged in $\sqrt{5} \times \sqrt{5}$ ordering [19]. As depicted in Fig. 3(e), the unit cell of the vacancy-ordered Fe_4Se_5 lattice is consistent with the $(\sqrt{5} \times \sqrt{5})$-$R26.6^\circ$ supercell of FeSe and naturally has two equivalent orientations that lead to two kinds of domains in the films. Interestingly, Fe_4Se_5 is an antiferromagnetic insulator [19], also consistent with recent observations on as-grown multilayer FeSe films on STO [29].

Depositing Fe onto this $\sqrt{5} \times \sqrt{5}$ surface recovered the structure to 1 × 1 FeSe [Figs. 4(a) and 4(b)]. The (01) diffraction streak intensity increased by ∼60% when reaching the maximum at $t_{\text{Fe}} = 364$ s [Fig. 4(c)] and the $\sqrt{5} \times \sqrt{5}$ order disappeared during the deposition [Fig. 4(b)]. Note that the deposition time t_{Fe} here is much longer than that for the 1-UC films [Fig. 1(d)], indicating that the Fe vacancies existed not only in the top layer but also in the whole film, and the Fe atoms diffused into the bottom layers. With $t_{\text{FeSe}} = 25$ min for the initial growth of 5-UC $Fe_{1-\delta}Se$ film, $\delta = t_{\text{Fe}}/(t_{\text{FeSe}} + t_{\text{Fe}}) = 0.195$, close to the vacancy density in Fe_4Se_5 ($\delta = 0.2$).

Intriguingly, this process is reversible by alternating the deposition of Fe and Se atoms. We carried out cycles of Se and Fe deposition on the same sample [Fig. 4(c)] and found that the film switched between two phases: the $\sqrt{5} \times \sqrt{5}$ order as shown in Fig. 4(a) after Se deposition and the 1 × 1 order as shown in Fig. 4(b) after Fe deposition. The 5-UC film after two cycles of Se-Fe deposition still showed superconductivity

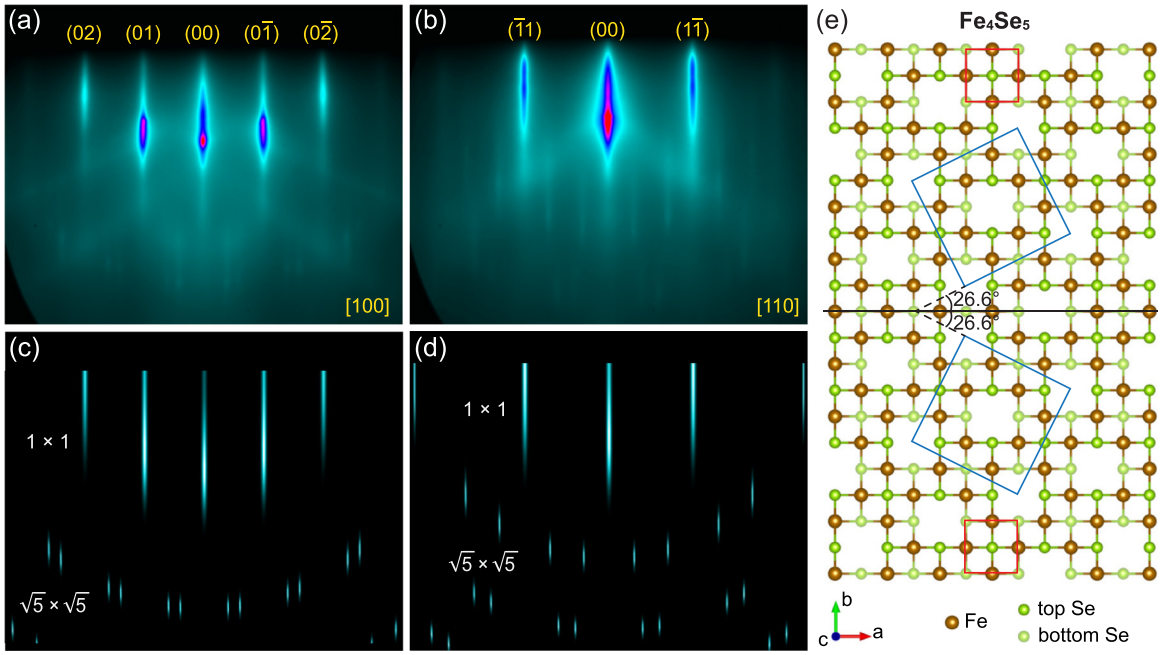

FIG. 3. (a) and (b) RHEED images of $\sqrt{5} \times \sqrt{5}$ 5-UC Fe_xSe film with the electron beam along the [100] and [110] directions, respectively. (c) and (d) Simulated RHEED patterns of a 1 × 1 square lattice with two ($\sqrt{5} \times \sqrt{5}$)-R26.6° supercells, with the electron beam in the [100] and [110] directions, respectively. (e) Sketched lattice structure of Fe-vacancy phase Fe_4Se_5 with two possible domains [19]. The red and blue squares indicate the unit cells of FeSe and Fe_4Se_5, respectively.

in transport measurement with $T_c^{mid} = 18$ K [Fig. 4(d)]. The possible causes of the lower T_c include the following: (1) the T_c of FeSe on STO decreases with increasing film thickness [13]; (2) for multilayer FeSe on STO, only the bottom layer can be superconducting [3,30], and it is more difficult for Fe atoms to penetrate the top layers to completely restore the stoichiometry of the bottom layer. Nevertheless, the results of the 5-UC film show that our method can control the stoichiometry of FeSe in a straightforward fashion, and demonstrate that the stoichiometry of FeSe films plays a key role in the emergence of superconductivity.

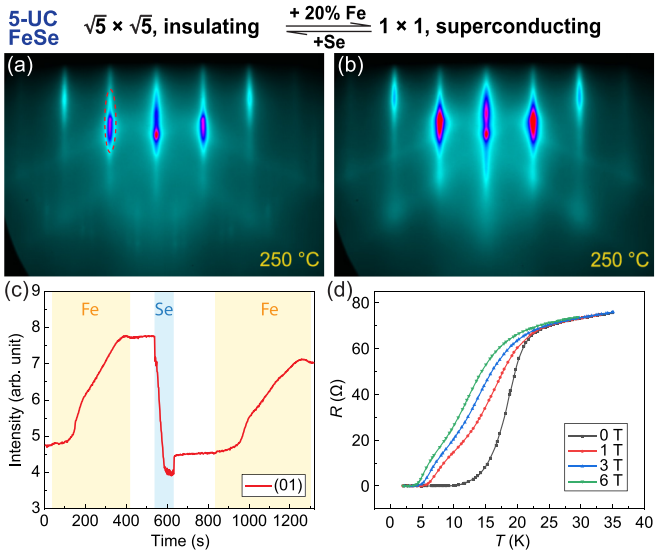

FIG. 4. (a) and (b) RHEED images of Se-added and Fe-adjusted 5-UC FeSe films, respectively. (c) Integrated intensity of (01) diffraction streaks in the elliptical area in (a), as a function of time. The yellow and blue intervals indicate the periods of Fe and Se deposition, respectively. The Se/Fe flux ratio was ∼5. (d) Temperature dependence of the resistance of the 5-UC FeSe film after two cycles of Se-Fe deposition, with different out-of-plane magnetic field.

Figure 5 summarizes the transport data of multiple 1- and 2-UC FeSe films on STO. The as-grown film is not superconducting, while all the other films, whether treated by annealing or Fe deposition or a combination of both, share similar superconducting transition temperatures. Although the transition widths differ (most likely due to different homogeneity of the films), the T_c^{mid}, which reflects the average T_c of the entire sample, falls in a narrow range of 22–24 K. This again manifests that the essence of the annealing process is increasing the Fe content in Fe_xSe toward $x = 1$. We note that x could be above 1 if Fe atoms are overdeposited, but the excess Fe on FeSe films, if any, will react with Te during the growth of FeTe capping layers. As magnetic impurities, excess Fe atoms would strongly suppress the superconductivity [31]. Therefore, the superconducting FeSe films showing optimal T_c, either annealed or Fe adjusted, should be close to stoichiometry.

It has been widely accepted that electrons doping to the FeSe film play a critical role in determining the superconducting properties [4,32]. Oxygen vacancies dope the STO surface and provide electrons for FeSe films through interfacial charge transfer [33,34]. They are usually generated during the thermal treatment of STO in vacuum [25,35]. Since we have made the FeSe films superconducting without long-time annealing, we argue that the oxygen vacancies are not primarily generated in the annealing process of the film but in the pretreatments of the STO substrates where the temperature is much higher than the annealing temperature

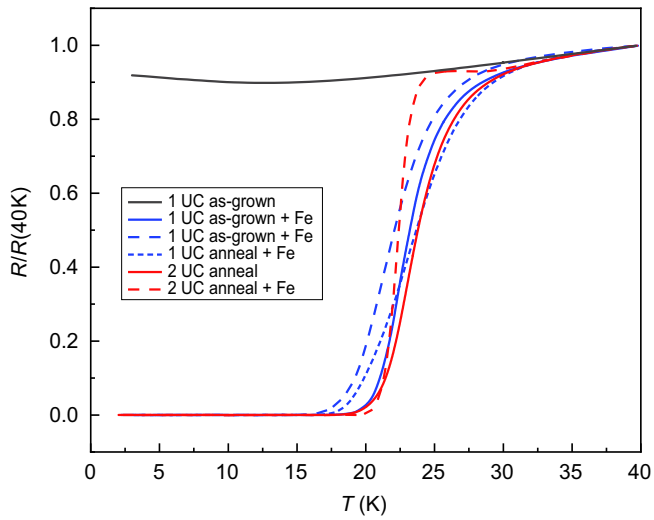

FIG. 5. Summary of transport measurement results of different samples. The anneal was carried out at 480 °C for 3 h. All samples were capped by 12-UC FeTe.

for FeSe. However, the insulating gap of as-grown FeSe could prevent the electrons in STO from transferring over. Hence the increase of electron concentration observed in FeSe films during annealing [4] is a result of the removal of Fe vacancies that act as hole dopants, in cooperation with the activation of the charge transfer from the STO.

Various mechanisms might contribute to the restoration of superconductivity upon reaching stoichiometry. A previous study observed that when the annealing is insufficient, surface doping by potassium cannot induce well-defined superconductivity [36], which is in contrast to Fe deposition, implying that tuning the stoichiometry has more effects than charge doping. Magnetic exchange bias effect measurements provided evidence for antiferromagnetic order in as-grown FeSe films, which becomes absent after annealing [29]. The dissolution of the magnetic order may be a hint to the spin fluctuation, one of the proposed pairing mechanisms for FeSe [32], which has shown signatures in scanning tunneling spectroscopy (STS) [8,9]. Furthermore, STS also showed that Fe vacancies destroy the superconducting gap and induce bound states [37]. By removing these defects with annealing or Fe deposition, the pair-breaking scattering of the Cooper pairs is minimized. Multiple factors need to be considered in future studies to interpret the emergence of superconductivity in FeSe thin films.

Since its discovery in 2012, FeSe/STO superconductor has drawn great attention to its particular properties that are distinct from the bulk, e.g., the high T_c, the electron doping, and the interface electron-phonon coupling. Our work reveals the similarity of FeSe thin film to the bulk in terms of stoichiometry-controlled phase transition. We have successfully tuned the composition of few-layer FeSe films on STO by selective deposition of Fe or Se. The as-grown or Se-rich phase has Fe vacancies up to 20% and is insulating, while the metallic/superconducting phase is close to stoichiometric, which can be achieved by either high-temperature annealing or deposition of a proper amount of Fe. Only when proper stoichiometry is reached can interfacial effects produce the superconductivity with high T_c. Our work unveils the essence of the annealing and highlights the crucial role of stoichiometry in the properties of FeSe on $SrTiO_3$.

We thank Bruce A. Davidson for fruitful discussions. This research was supported by the Max Planck-UBC-UTokyo Centre for Quantum Materials, by the Canada First Research Excellence Fund, Quantum Materials and Future Technologies Program, by Natural Sciences and Engineering Research Council of Canada (NSERC), and by Canada Foundation for Innovation (CFI).

[1] H. Hosono and K. Kuroki, Phys. C (Amsterdam, Neth.) **514**, 399 (2015).
[2] F.-C. Hsu, J.-Y. Luo, K.-W. Yeh, T.-K. Chen, T.-W. Huang, P. M. Wu, Y.-C. Lee, Y.-L. Huang, Y.-Y. Chu, D.-C. Yan, and M.-K. Wu, Proc. Natl. Acad. Sci. USA **105**, 14262 (2008).
[3] Q.-Y. Wang, Z. Li, W.-H. Zhang, Z.-C. Zhang, J.-S. Zhang, W. Li, H. Ding, Y.-B. Ou, P. Deng, K. Chang, J. Wen, C.-L. Song, K. He, J.-F. Jia, S.-H. Ji, Y.-Y. Wang, L.-L. Wang, X. Chen, X.-C. Ma, and Q.-K. Xue, Chin. Phys. Lett. **29**, 037402 (2012).
[4] S. He, J. He, W. Zhang, L. Zhao, D. Liu, X. Liu, D. Mou, Y. B. Ou, Q. Y. Wang, Z. Li, L. Wang, Y. Peng, Y. Liu, C. Chen, L. Yu, G. Liu, X. Dong, J. Zhang, C. Chen, Z. Xu, X. Chen, X. Ma, Q. Xue, and X. J. Zhou, Nat. Mater. **12**, 605 (2013).
[5] S. Tan, Y. Zhang, M. Xia, Z. Ye, F. Chen, X. Xie, R. Peng, D. Xu, Q. Fan, H. Xu, J. Jiang, T. Zhang, X. Lai, T. Xiang, J. Hu, B. Xie, and D. Feng, Nat. Mater. **12**, 634 (2013).
[6] D. Huang and J. E. Hoffman, Annu. Rev. Condens. Matter Phys. **8**, 311 (2017).
[7] C. Liu and J. Wang, 2D Mater. **7**, 022006 (2020).
[8] C. Liu, Z. Wang, S. Ye, C. Chen, Y. Liu, Q. Wang, Q. H. Wang, and J. Wang, Nano Lett. **19**, 3464 (2019).
[9] C. Liu, Z. Wang, Y. Gao, X. Liu, Y. Liu, Q. H. Wang, and J. Wang, Phys. Rev. Lett. **123**, 036801 (2019).
[10] Z. Li, J. P. Peng, H. M. Zhang, W. H. Zhang, H. Ding, P. Deng, K. Chang, C. L. Song, S. H. Ji, L. Wang, K. He, X. Chen, Q. K. Xue, and X. C. Ma, J. Phys.: Condens. Matter **26**, 265002 (2014).
[11] C.-L. Song, Y.-L. Wang, Y.-P. Jiang, Z. Li, L. Wang, K. He, X. Chen, X.-C. Ma, and Q.-K. Xue, Phys. Rev. B **84**, 020503(R) (2011).
[12] W. Zhang, Z. Li, F. Li, H. Zhang, J. Peng, C. Tang, Q. Wang, K. He, X. Chen, L. Wang, X. Ma, and Q.-K. Xue, Phys. Rev. B **89**, 060506(R) (2014).
[13] Q. Wang, W. Zhang, Z. Zhang, Y. Sun, Y. Xing, Y. Wang, L. Wang, X. Ma, Q.-K. Xue, and J. Wang, 2D Mater. **2**, 044012 (2015).
[14] W. Schuster, H. Mikler, and K. L. Komarek, Monatsh. Chem. **110**, 1153 (1979).

[15] T. M. McQueen, Q. Huang, V. Ksenofontov, C. Felser, Q. Xu, H. Zandbergen, Y. S. Hor, J. Allred, A. J. Williams, D. Qu, J. Checkelsky, N. P. Ong, and R. J. Cava, Phys. Rev. B **79**, 014522 (2009).

[16] A. J. Williams, T. M. McQueen, and R. J. Cava, Solid State Commun. **149**, 1507 (2009).

[17] C. Koz, M. Schmidt, H. Borrmann, U. Burkhardt, S. Rößler, W. Carrillo-Cabrera, W. Schnelle, U. Schwarz, and Y. Grin, Z. Anorg. Allg. Chem. **640**, 1600 (2014).

[18] S. Rößler, C. Koz, L. Jiao, U. K. Rößler, F. Steglich, U. Schwarz, and S. Wirth, Phys. Rev. B **92**, 060505(R) (2015).

[19] T. K. Chen, C. C. Chang, H. H. Chang, A. H. Fang, C. H. Wang, W. H. Chao, C. M. Tseng, Y. C. Lee, Y. R. Wu, M. H. Wen, H. Y. Tang, F. R. Chen, M. J. Wang, M. K. Wu, and D. Van Dyck, Proc. Natl. Acad. Sci. USA **111**, 63 (2014).

[20] F. Li, Q. Zhang, C. Tang, C. Liu, J. Shi, C. Nie, G. Zhou, Z. Li, W. Zhang, C.-L. Song, K. He, S. Ji, S. Zhang, L. Gu, L. Wang, X.-C. Ma, and Q.-K. Xue, 2D Mater. **3**, 024002 (2016).

[21] D. Huang, T. A. Webb, C.-L. Song, C.-Z. Chang, J. S. Moodera, E. Kaxiras, and J. E. Hoffman, Nano Lett. **16**, 4224 (2016).

[22] Y. Hu, Y. Xu, Q. Wang, L. Zhao, S. He, J. Huang, C. Li, G. Liu, and X. J. Zhou, Phys. Rev. B **97**, 224512 (2018).

[23] W. Zhao, M. Li, C.-Z. Chang, J. Jiang, L. Wu, C. Liu, J. S. Moodera, Y. Zhu, and M. H. W. Chan, Sci. Adv. **4**, eaao2682 (2018).

[24] W.-H. Zhang, Y. Sun, J.-S. Zhang, F.-S. Li, M.-H. Guo, Y.-F. Zhao, H.-M. Zhang, J.-P. Peng, Y. Xing, H.-C. Wang, T. Fujita, A. Hirata, Z. Li, H. Ding, C.-J. Tang, M. Wang, Q.-Y. Wang, K. He, S.-H. Ji, X. Chen, J.-F. Wang, Z.-C. Xia, L. Li, Y.-Y. Wang, J. Wang, L.-L. Wang, M.-W. Chen, Q.-K. Xue, and X.-C. Ma, Chin. Phys. Lett. **31**, 017401 (2014).

[25] K. Zou, S. Mandal, S. D. Albright, R. Peng, Y. Pu, D. Kumah, C. Lau, G. H. Simon, O. E. Dagdeviren, X. He, I. Božović, U. D. Schwarz, E. I. Altman, D. Feng, F. J. Walker, S. Ismail-Beigi, and C. H. Ahn, Phys. Rev. B **93**, 180506(R) (2016).

[26] M.-L. Zhang, J.-F. Ge, M.-C. Duan, G. Yao, Z.-L. Liu, D.-D. Guan, Y.-Y. Li, D. Qian, C.-H. Liu, and J.-F. Jia, Acta Phys. Sin. **65**, 127401 (2016).

[27] P. K. Maheshwari, R. Jha, B. Gahtori, and V. P. S. Awana, J. Supercond. Nov. Magn. **28**, 2893 (2015).

[28] Y. Fang, D. H. Xie, W. Zhang, F. Chen, W. Feng, B. P. Xie, D. L. Feng, X. C. Lai, and S. Y. Tan, Phys. Rev. B **93**, 184503 (2016).

[29] Y. Zhou, L. Miao, P. Wang, F. F. Zhu, W. X. Jiang, S. W. Jiang, Y. Zhang, B. Lei, X. H. Chen, H. F. Ding, H. Zheng, W. T. Zhang, J. F. Jia, D. Qian, and D. Wu, Phys. Rev. Lett. **120**, 097001 (2018).

[30] X. Liu, D. Liu, W. Zhang, J. He, L. Zhao, S. He, D. Mou, F. Li, C. Tang, Z. Li, L. Wang, Y. Peng, Y. Liu, C. Chen, L. Yu, G. Liu, X. Dong, J. Zhang, C. Chen, Z. Xu, X. Chen, X. Ma, Q. Xue, and X. J. Zhou, Nat. Commun. **5**, 5047 (2014).

[31] C. Liu, G. Wang, and J. Wang, J. Phys.: Condens. Matter **31**, 285002 (2019).

[32] D.-H. Lee, Annu. Rev. Condens. Matter Phys. **9**, 261 (2018).

[33] H. Zhang, D. Zhang, X. Lu, C. Liu, G. Zhou, X. Ma, L. Wang, P. Jiang, Q. K. Xue, and X. Bao, Nat. Commun. **8**, 214 (2017).

[34] G. Gong, H. Yang, Q. Zhang, C. Ding, J. Zhou, Y. Chen, F. Meng, Z. Zhang, W. Dong, F. Zheng, P. Zhang, L. Yang, L. Gu, Q.-K. Xue, and L. Wang, Phys. Rev. B **100**, 224504 (2019).

[35] T. Nishimura, A. Ikeda, H. Namba, T. Morishita, and Y. Kido, Surf. Sci. **421**, 273 (1999).

[36] C. Tang, D. Zhang, Y. Zang, C. Liu, G. Zhou, Z. Li, C. Zheng, X. Hu, C. Song, S. Ji, K. He, X. Chen, L. Wang, X. Ma, and Q.-K. Xue, Phys. Rev. B **92**, 180507(R) (2015).

[37] C. Liu, J. Mao, H. Ding, R. Wu, C. Tang, F. Li, K. He, W. Li, C.-L. Song, X.-C. Ma, Z. Liu, L. Wang, and Q.-K. Xue, Phys. Rev. B **97**, 024502 (2018).